Carbohydrate Polymers 288 (2022) 119373

Contents lists available at ScienceDirect

Carbohydrate Polymers

journal homepage: www.elsevier.com/locate/carbpol

Extending the diversity of *Myceliophthora thermophila* LPMOs: Two different xyloglucan cleavage profiles

Peicheng Sun, Melanie de Munnik, Willem J.H. van Berkel, Mirjam A. Kabel *

Laboratory of Food Chemistry, Wageningen University & Research, Bornse Weilanden 9, 6708, WG, Wageningen, the Netherlands

ARTICLE INFO

Keywords:
Lignocellulose
Xyloglucan
LPMOs
Active site segment
Oxidative cleavage
Reduction
Mass spectrometric fragmentation

ABSTRACT

Lytic polysaccharide monooxygenases (LPMOs) play a key role in enzymatic conversion of plant cell wall polysaccharides. Continuous discovery and functional characterization of LPMOs highly contribute to the tailor-made design and improvement of hydrolytic-activity based enzyme cocktails. In this context, a new *Mt*LPMO9F was characterized for its substrate (xyloglucan) specificity, and *Mt*LPMO9H was further delineated. Aided by sodium borodeuteride reduction and hydrophilic interaction chromatography coupled to mass spectrometric analysis, we found that both *Mt*LPMOs released predominately C4-oxidized, and C4/C6-double oxidized xylogluco-oligosaccharides. Further characterization showed that *Mt*LPMO9F, having a short active site segment 1 and a long active site segment 2 ($^{-}$Seg1^{+}Seg2), followed a "substitution-intolerant" xyloglucan cleavage profile, while for *Mt*LPMO9H ($^{+}$Seg1^{-}Seg2) a "substitution-tolerant" profile was found. The here characterized xyloglucan specificity and substitution (in)tolerance of *Mt*LPMO9F and *Mt*LPMO9H were as predicted according to our previously published phylogenetic grouping of AA9 LPMOs based on structural active site segment configurations.

1. Introduction

Lignocellulose-based biorefineries have lately attracted interest to replace fossil based refineries (Cherubini, 2010; Nanda, Mohammad, Reddy, Kozinski, & Dalai, 2014). An important process step in these biorefineries is the enzymatic release of fermentable monosaccharides from lignocellulosic hemicellulose and cellulose (Himmel et al., 2007; Merino & Cherry, 2007; Straathof, 2014). Traditionally, only hydrolytic enzymes were considered relevant for hemicellulose and cellulose degradation activity, and are, therefore, the basis of commercial enzyme cocktails (Gao et al., 2011; Payne et al., 2015). In the last decade, the composition of these cocktails benefit from the discovery of lytic polysaccharide monooxygenases (LPMOs), which have been shown to greatly enhance hydrolytic conversion of hemicellulose and cellulose (Cannella, Chia-wen, Felby, & Jørgensen, 2012; Forsberg et al., 2011; Harris et al., 2010; Karnaouri et al., 2017). Continuous discovery and functional characterization of novel LPMOs is expected to highly contribute to future application-tailored hydrolytic-activity based enzyme cocktails. In this context, in our research, we aim to understand the role of LPMOs discovered in the genome of the thermophilic fungus *Myceliophthora thermophila* C1 (*Mt*) (Berka et al., 2011; Hinz et al., 2009).

LPMOs are mono-copper dependent redox enzymes and currently classified into sequence-based "Auxiliary Activity" families (AA) 9–11 and 13–17 in the Carbohydrate-Active enZymes (CAZy) database (http://www.cazy.org) (Lombard, Ramulu, Drula, Coutinho, & Henrissat, 2014; Sabbadin et al., 2021). The fungal AA9 family constitutes the largest LPMO family (Berka et al., 2011). AA9 members catalyze the

Abbreviations: LPMO, lytic polysaccharide monooxygenase; *Mt*, *Myceliophthora thermophila* C1; AA, Auxiliary Activities; CAZy, Carbohydrate-Active enZymes; Seg, active site segment; TXG, tamarind xyloglucan; $NaBD_4$, sodium borodeuteride; HILIC-ESI-CID-MS/MS^2, hydrophilic interaction chromatography–electrospray ionization–collision induced dissociation–mass spectrometry; RAC, regenerated amorphous cellulose; Asc, ascorbic acid; AEC, anion exchange chromatography; SEC, size exclusion chromatography; CEC, cation exchange chromatography; SDS-PAGE, sodium dodecyl sulfate–polyacrylamide gel electrophoresis; HPAEC-PAD, high performance anion exchange chromatography with pulsed amperometric detection; SPE, solid phrase extraction; DP, degree of polymerization; PASC, phosphoric acid swollen cellulose; BC, bacterial cellulose; Gn, non-oxidized cello-oligosaccharides and "n" for the number of hexaoses; C4ox, C4-oxidized products; C1ox, C1-oxidized products; C4C6ox, C4/C6-double oxidized products; RD, reduced; H_nP_m, "H" for "hexaose", "P" for "pentaose", "n" for the number of hexaoses and "m" for the number of pentaoses; CBM, carbohydrate binding module.

* Corresponding author.
E-mail addresses: peicheng.sun@wur.nl (P. Sun), willem.vanberkel@wur.nl (W.J.H. van Berkel), mirjam.kabel@wur.nl (M.A. Kabel).

https://doi.org/10.1016/j.carbpol.2022.119373
Received 14 January 2022; Received in revised form 14 March 2022; Accepted 15 March 2022
Available online 18 March 2022

Table 1
Partially characterized AA9 LPMOs from *M. thermophila*.[a]

LPMO name	UniProt ID	Active site segment configuration	Substrate specificity	Xyloglucan specificity	References
*Mt*LPMO9A	G2QNT0	$^{-}$Seg1^{-}Seg2[b]	Cellulose (RAC), xylan associated to RAC, xyloglucan[c], mixed β-(1→3, 1→4)-linked glucan	Active[c]	(Frommhagen et al., 2015)
*Mt*LPMO9L	Unknown	$^{-}$Seg1^{-}Seg2[b]	Cellulose (PASC, Avicel)	Inactive	(Zhou et al., 2019)
MYCTH_112089	G2QI82	$^{-}$Seg1^{-}Seg2[b]	Cellulose (PASC)[d]	n.d.	(Vu, Beeson, Phillips, Cate, & Marletta, 2014)
*Mt*LPMO9B	G2QCJ3	$^{-}$Seg1^{+}Seg2^{+}Seg3	Cellulose (RAC, Avicel, BC)	Inactive	(Frommhagen et al., 2016; Grieco et al., 2020; Sun et al., 2021)
*Mt*LPMO9I	G2Q774	$^{-}$Seg1^{+}Seg2^{+}Seg3	Cellulose (RAC, Avicel)	Inactive	(Sun, Frommhagen, et al., 2020)
*Mt*LPMO9C	G2QA92	$^{-}$Seg1^{+}Seg2	Cellulose (RAC), xyloglucan[e], mixed β-(1→3, 1→4)-linked glucan	n.d.	(Frommhagen, van Erven, et al., 2017)
*Mt*LPMO9E (*Mt*LPMO9J)	G2Q7A5	$^{-}$Seg1^{+}Seg2	Cellulose (RAC, Avicel), xyloglucan, cello-oligosaccharides (DP ≥ 5)	Substitution-intolerant	(Kadowaki et al., 2018; Sun, Frommhagen, et al., 2020)
*Mt*LPMO9D	G2QAB5	$^{+}$Seg1^{-}Seg2	Cellulose (RAC)[d]	n.d.	(Frommhagen, Westphal, et al., 2017)
*Mt*LPMO9H	G2Q9T3	n.d.	Cellulose (RAC, Avicel)[d]	n.d.	(Grieco et al., 2020; Karnaouri et al., 2017; Sun et al., 2021; Sun et al., 2022)

[a] Abbreviations: RAC, regenerated amorphous cellulose; PASC, phosphoric acid swollen cellulose; BC, bacterial cellulose; n.d., not determined.
[b] Based on the reported short L3 loop and L2 loop.
[c] Trace of activity towards xyloglucan, too low to determine the xyloglucan specificity.
[d] Only cellulose was tested.
[e] Data was not conclusive to determine xyloglucan specificity.

regioselective C1- and/or C4-oxidative cleavage of cellulose using molecular oxygen (O_2) and/or hydrogen peroxide (H_2O_2) and an external electron donor as co-substrates (Bissaro, Varnai, Rohr, & Eijsink, 2018; Hangasky, Iavarone, & Marletta, 2018). C1-oxidative cleavage results in δ-lactones, which convert to aldonic acids in aqueous solutions, while C4-oxidative cleavage forms 4-ketoaldoses. These C4-ketones are in equilibrium with their geminal diol form in aqueous solutions, although the equilibrium will majorly be on the ketone side (Beeson, Phillips, Cate, & Marletta, 2012; Isaksen et al., 2014). Recently, we showed that C4 cellulose oxidation can be accompanied by C6-oxidation, based on identified double, C4 and C6, oxidized cello-oligosaccharides (Sun et al., 2022). Although the regioselectivity of LPMOs is not fully understood, it has been proposed that it may reflect how LPMOs bind to their substrates (Frandsen & Lo Leggio, 2016; Simmons et al., 2017; Vaaje-Kolstad, Forsberg, Loose, Bissaro, & Eijsink, 2017). The latter might also reflect their substrate specificity, as was concluded from structure-based (e.g., active site segment (Seg) based) multiple sequence alignment of AA9 LPMOs (Laurent et al., 2019; Sun, Laurent, et al., 2020). This analysis indicated three major groups: i) cellulose-specific LPMOs ("short Seg1 & short Seg2" ($^{-}$Seg1^{-}Seg2) and "short Seg1 & long Seg2 & long Seg3" ($^{-}$Seg1^{+}Seg2^{+}Seg3)), ii) cellulose and xyloglucan (substitution-intolerant) active LPMOs ($^{-}$Seg1^{+}Seg2), iii) cellulose and xyloglucan (substitution-tolerant) active LPMOs ($^{+}$Seg1^{-}Seg2). Although in that work, a number of candidates were shown to have the named specificities, only one *Mt*LPMO has been studied for its xyloglucan specificity (Table 1). For the other eight partially characterized AA9 *Mt*LPMOs out of twenty-two present in the genome, and for yet uncharacterized *Mt*LPMOs, xyloglucan specificity needs to be unraveled.

Xyloglucan is a heteropolysaccharide composed of a cellulose-like β-(1→4) linked-D-glucosyl backbone. The glucosyl residues can be substituted by a D-xylosyl residue via α-(1→6) linkages (Caffall & Mohnen, 2009; Hoffman et al., 2005; McNeil, Darvill, Fry, & Albersheim, 1984). The unsubstituted and D-xylosyl substituted glucosyl units are coded as "G" and "X" based on the one-letter nomenclature developed by Fry et al. (1993). The D-xylosyl residues can be even further substituted with β-(1→2) linked D-galactosyl residues (coded "L"). Other substitutions are less common and described elsewhere (Fry et al., 1993). The most common xyloglucan structure is built by so-called "XXXG-" and "XXGG-type" block-wise units (Vincken, York, Beldman, & Voragen, 1997). For instance, tamarind xyloglucan (TXG) is constructed by the repeated "XXXG-type" units with partially substituted galactosyl residues (XLXG, XXLG and XLLG) (Fry et al., 1993).

In this work, it is hypothesized that the configuration of active site segments of AA9 LPMOs can be used to predict their xyloglucan cleavage profiles. To prove this hypothesis, a new *Mt*LPMO9F and a partially characterized *Mt*LPMO9H were studied for their active site configuration, and produced for characterization of their regioselectivity and substrate specificity with a focus on oxidative cleavage patterns of xyloglucan. *Mt*LPMO9F- and *Mt*LPMO9H-generated C4-oxidized xyloglucan-oligosaccharides, and double C4/C6-oxidized ones, were identified in detail by using sodium borodeuteride ($NaBD_4$) reduction and hydrophilic interaction chromatography–electrospray ionization–collision induced dissociation–mass spectrometry (HILIC-ESI-CID-MS/MS^2).

2. Materials and methods

2.1. Carbohydrates, cellulose substrate and other chemicals

$NaBD_4$ and ammonium acetate were purchased from Sigma-Aldrich (St. Louis, Missouri, USA). Xyloglucan from tamarind (*Tamarindus indica*, TXG), TXG oligosaccharide standard (xyloglucan hepta-, octa- and nona-saccharides), cellobiose, cellotriose, cellotetraose, cellopentaose and cellohexaose were purchased from Megazyme (Bray, Ireland). Regenerated amorphous cellulose (RAC) was prepared from Avicel® PH-101 (Sigma-Aldrich) as described previously (Frommhagen et al., 2015). Ascorbic acid (Asc) was purchased from VWR International (Radnor, Pennsylvania, USA). Water used in all experiments was produced by a Milli-Q system (Millipore, Molsheim, France). Other carbohydrates used for substrate screening were purchased from either Sigma-Aldrich or Megazyme.

2.2. Structure-based multiple sequence alignment

Amino acid sequences of *Mt*LPMO9F (MYCTH_111088, UniProt ID: G2Q9F7) and *Mt*LPMO9H (MYCTH_46583, UniProt ID: G2Q9T3), together with previously studied *Nc*LPMO9C, *Mt*LPMO9E, *Nc*LPMO9M (Sun, Laurent, et al., 2020) and *Fg*LPMO9A (Nekiunaite et al., 2016) were fine-tuned by removing the signal peptide, the linker- and the CBM-domain as described previously (Sun, Laurent, et al., 2020). Subsequently, a structure-based multiple sequence alignment was performed with these six AA9 LPMOs. The resulting structure-based alignment was further divided into regions "Segments 1 to 5" (Seg1–Seg5) as described previously (Sun, Laurent, et al., 2020), which was used to determine the short and/or long segments.

Table 2
Carbohydrate substrate specificity screening of *Mt*LPMO9F and *Mt*LPMO9H.

Occurrence of oxidative cleavage (+) or not (−) in the presence of 1 mM Asc		
Substrate	*Mt*LPMO9F	*Mt*LPMO9H
Cellulose		
RAC	+	+
Bacterial cellulose	+	+
Avicel® PH-101	+	+
Carboxymethyl cellulose	+	+
Hemicellulose		
Xyloglucan (tamarind)	+	+
Mixed β-(1→3, 1→4)-linked glucan (barley)	+	−
Mixed β-(1→3, 1→4)-linked glucan (oat spelt)	+	−
Xylan (oat spelt)	−	−
Xylan (birchwood)	−	−
Arabinoxylan (wheat)	−	−
Mannan (acacia)	−	−
Galactan (potato)	−	−
Glucomannan (konjac)	+	−
Arabinan (sugar beet)	−	−
Laminarin (*Laminaria digitata*)	−	−
RAC/hemicellulose combination		
RAC + Xyloglucan (tamarind)	+[a]	+[a]
RAC + Xylan (birchwood)	+[b]	+[b]
Oligosaccharides		
Cellopentaose	+	−
Cellohexaose	+	−
Xylo-oligosaccharides (DP2–6)	−	−
Others		
Chitin (shrimp shells)	−	−
Starch (maize)	−	−

[a] Oxidative cleavage towards both RAC and xyloglucan.
[b] Oxidative cleavage only towards RAC.

2.3. Expression, production and purification of MtLPMO9F and MtLPMO9H

The gene encoding *Mt*LPMO9F was homologously expressed in a low protease/low hemicellulase/low cellulase producing *Myceliophthora thermophila* C1 strain by IFF Nutrition & Biosciences (Leiden, The Netherlands), essentially as described elsewhere (Punt et al., 2010; Visser et al., 2011). The expression, production and purification of *Mt*LPMO9H have been described previously (Sun et al., 2021).

*Mt*LPMO9F was purified by four subsequent chromatographic steps. Crude *Mt*LPMO9F-rich fermentation broth was filtrated and dialyzed against 10 mM potassium phosphate buffer pH 7.6 before chromatographic purification. The dialyzed *Mt*LPMO9F was purified by step-wise anion exchange chromatography (AEC), size exclusion chromatography (SEC) and cation exchange chromatography (CEC). Columns used, purification settings and elution program of AEC, SEC and CEC have been described previously (Sun et al., 2021). The purest third step CEC-purified *Mt*LPMO9F-containing fractions based on sodium dodecyl sulfate–polyacrylamide gel electrophoresis (SDS-PAGE) were further purified by the fourth-step CEC on an ÄKTA-Micro preparative chromatography system (GE Healthcare). Settings and elution program used in this last CEC purification step of *Mt*LPMO9F was the same as described for the last CEC purification step of *Mt*LPMO9H (Sun et al., 2021). All fractions were collected and immediately stored on ice. Peak fractions based on UV 280 nm were adjusted to an approximate concentration of 2 mg/mL determined by BCA assay and analyzed by SDS-PAGE, as described previously (Sun, Frommhagen, et al., 2020) to determine their purity. *Mt*LPMO9F fractions with the highest purity based on SDS-PAGE were frozen in liquid nitrogen and stored at −80 °C.

2.4. Generation of carbohydrate digests by MtLPMO9F and MtLPMO9H

Carbohydrates listed in Table 2 were mixed with 50 mM ammonium acetate buffer (pH 5.0) to a concentration of 2 mg/mL. For RAC and hemicellulose combination, each type was 2 mg/mL. Subsequently, 2 μM of *Mt*LPMO9F or *Mt*LPMO9H corrected by impurities based on SDS-PAGE results in Fig. A.1 was added to the corresponding carbohydrate mixture containing 1 mM Asc (final concentration). Control reactions were performed in the absence of Asc. All reactions containing 500 μL total volume were incubated at 30 °C by using an Eppendorf Thermomixer® comfort, placed in an almost vertical direction, at 800 rpm for 24 h in duplicate. The reactions were stopped by immediately separating supernatants after centrifugation at 22000 ×*g* for 10 min at 4 °C in a table centrifuge. The resulting supernatants were collected and diluted five times for high performance anion exchange chromatography with pulsed amperometric detection (HPAEC-PAD) analysis.

Part of supernatants from RAC and TXG digests were reduced by $NaBD_4$ followed by solid phase extraction (SPE) as described in Section 2.5. A cello-oligosaccharide standard mixture containing cellobiose, cellotriose, cellotetraose, cellopentaose and cellohexaose (1 μg/mL each) and a TXG oligosaccharide standard (20 μg/mL) were also analyzed by HPAEC-PAD.

2.5. Reduction of generated oxidized cello- and xylogluco-oligosaccharides with $NaBD_4$ and clean-up with SPE

Reduction was performed by adding 200 μL freshly prepared 0.5 M $NaBD_4$ to 200 μL of i) the cello-oligosaccharide standard mixture (50 μg/mL of each degree of polymerization (DP)), ii) 100 μg/mL of TXG oligosaccharide standard and iii) supernatants obtained from the *Mt*LPMO9F- and *Mt*LPMO9H-RAC or TXG digests at 20 °C for 20 h. A clean-up procedure for reduced digests was carried out by using SPE with Supelclean™ ENVI-Carb™ columns (3 mL, Sigma-Aldrich) as described previously (Sun, Frommhagen, et al., 2020). The dried reduced RAC and TXG digests were dissolved in 60% (v/v) acetonitrile in water. The reduced RAC and TXG digests were directly used for HILIC-ESI-CID-MS/MS^2 analysis or diluted twenty times for HPAEC-PAD analysis.

2.6. Analytic methods

2.6.1. HPAEC-PAD analysis for profiling oligosaccharides

All samples, including the non-reduced and reduced cello-oligosaccharide standard mixture, the TXG oligosaccharide standard, RAC and TXG digests of *Mt*LPMO9F or *Mt*LPMO9H, were analyzed by HPAEC-PAD with an ICS-5000 system (Dionex, Sunnyvale, California, USA) equipped with a CarboPac PA-1 column (2 mm ID × 250 mm; Dionex) in combination with a CarboPac PA guard column (2 mm ID × 50 mm; Dionex). The two mobile phases were (A) 0.1 M NaOH and (B) 1 M NaOAc in 0.1 M NaOH and the elution profile used has been described previously (Sun et al., 2021). HPAEC data was processed by using Chromeleon 7.2.10 software (Thermo Fisher Scientific, Waltham, Massachusetts, USA).

2.6.2. HILIC-ESI-CID-MS/MS^2 for elucidating the reduced oligosaccharide structures

Reduced forms of the cello-oligosaccharide standard mixture, the TXG oligosaccharide standard and digests of RAC and TXG were analyzed by using HILIC-ESI-CID-MS/MS^2. A Vanquish UHPLC system (Thermo Fisher Scientific) equipped with an Acquity UPLC BEH Amide column (Waters, Millford, Massachusetts, USA; 1.7 μm, 2.1 mm ID × 150 mm) and a VanGuard pre-column (Waters; 1.7 μm, 2.1 mm ID × 150 mm) was used. The column temperature was set at 35 °C under still air mode. Two mobile phases were used: water (A) and acetonitrile (B), both containing 0.1% (v/v) formic acid (FA) (all were UHPLC-grade; Biosolve, Valkenswaard, The Netherlands). The flow rate was set at 0.45 mL/min. The elution was performed as the following profile: 0–2 min at 82% B (isocratic), 2–62 min from 82% to 60% B (linear gradient), 62–62.5 min from 60% to 42% B (linear gradient), 62.5–69 min at 42% B (isocratic), 69–70 min from 42% to 82% B (linear gradient) and 70–80 min at 82% B (isocratic). Mass spectrometric data (*m/z*) were obtained

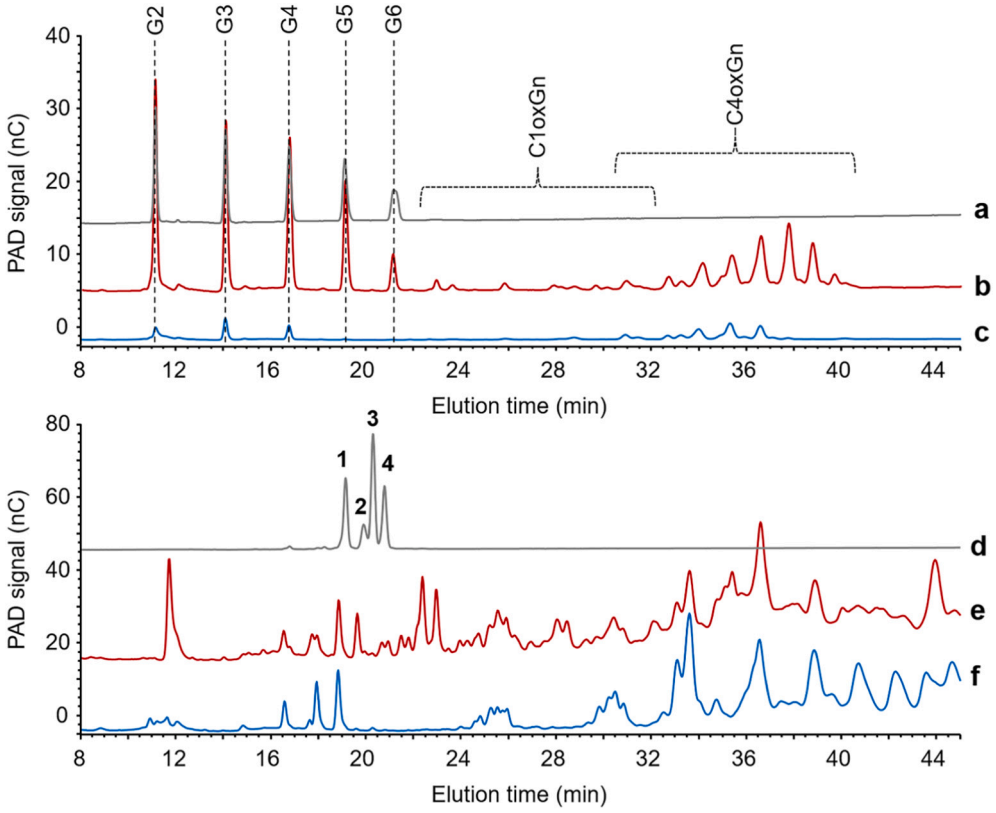

Fig. 1. HPAEC chromatograms of RAC (b and c) and TXG (e and f) digests generated by *Mt*LPMO9H (b and e) and *Mt*LPMO9F (c and f) in the presence of Asc. Cello-oligosaccharides standard mixture (a) and TXG oligosaccharide standard (d; 1 = XXXG, 2 = XLXG, 3 = XXLG and 4 = XLLG) are also shown. Control reactions are shown in Figs. A.3 and A.6.

by using an LTQ Velos Pro linear ion trap mass spectrometer (Thermo Fisher Scientific) equipped with a heated ESI probe coupled in-line to the UHPLC system as described above. MS data were collected in negative ionization mode with the following settings: source heater temperature 400 °C, capillary temperature 250 °C, sheath gas flow 50 units, source voltage 2.5 kV and *m/z* range 300–1500. As MS^2 settings, collision-induced dissociation (CID) was performed on the most intense product ion with a normalized collision energy of 35% and a minimum signal threshold of 10,000 counts. Activation Q and activation time were set at 0.25 and 10 ms, respectively. Mass spectrometric data were processed by using Xcalibur 4.3.73.11 software (Thermo Fisher Scientific).

3. Results and discussion

3.1. *MtLPMO9H and MtLPMO9F: active site segment configuration, substrate screening and cellulose regioselectivity*

To determine the configuration of active site segments (Seg1 to Seg5) of *Mt*LPM9H and *Mt*LPMO9F, their amino acid sequences were structurally-based aligned with four previously characterized AA9 LPMOs (Laurent et al., 2019; Sun, Laurent, et al., 2020). Based on the alignment shown in Fig. A.2, it was concluded that *Mt*LPMO9H has a long Seg1 and a short Seg2 ($^{+}$Seg1^{-}Seg2), similar to the configuration of *Nc*LPMO9M and *Fg*LPMO9A. In contrast, *Mt*LPMO9F holds a short Seg1 and a long Seg2 ($^{-}$Seg1^{+}Seg2), which is comparable to *Nc*LPMO9C and *Mt*LPMO9E. In our previous work, as outlined in the introduction, AA9 LPMOs with "$^{+}$Seg1^{-}Seg2" structural elements have been shown to oxidatively cleave cellulose in addition to xyloglucan via a "substitution-tolerant" cleavage behavior. AA9 LPMOs with "$^{-}$Seg1^{+}Seg2" structural elements have been shown to oxidatively cleave cellulose in addition to xyloglucan via a "substitution-intolerant" cleavage behavior. These correlations between configuration of active site segments and xyloglucan cleavage behaviors have also been shown in other studies (Chen, Zhang, Long, & Ding, 2021; Monclaro et al., 2020). To test the xyloglucan cleavage behaviors of *Mt*LPMO9F and *Mt*LPMO9H, first, an extensive substrate screening was performed (Table 2). Although *Mt*LPMO9H and *Mt*LPMO9F still contained a trace of cellulase impurity as judged from the enzyme incubations in the absence of Asc (Fig. A.3), LPMO-generated oxidized cello-oligosaccharides dominated (Fig. 1).

Overall, in the presence of Asc, *Mt*LPMO9H and *Mt*LPMO9F showed detectable oxidative cleavage of all four types of cellulose (Table 2). Based on the previously characterized LPMO-RAC profiles (Frommhagen et al., 2016; Sun, Frommhagen, et al., 2020), *Mt*LPMO9F released predominantly C4-oxidized cello-oligosaccharides from RAC (Fig. 1). Note that after $NaBD_4$ reduction and HILIC-ESI-CID-MS/MS^2 analysis, it was confirmed that *Mt*LPMO9F also generated a series of reduced C4/C6-double oxidized cello-oligosaccharides (RD-C4C6ox) (Fig. A.4) as has been shown for other AA9 LPMOs (Sun et al., 2022). As an example, the MS^2 fragmentation pattern of DP4 is presented in Fig. A.5. C1-oxidized cello-oligosaccharides were barely detected in the *Mt*LPMO9F-RAC digest.

In addition to cellulosic substrates, *Mt*LPMO9F also catalyzed the oxidative cleavage of xyloglucan (Fig. 1), mixed β-(1→3, 1→4)-linked β-glucan, glucomannan, cellopentaose and cellohexaose. Interestingly, the substrate specificity of *Mt*LPMO9F is comparable to that of *Nc*LPMO9C (Agger et al., 2014; Isaksen et al., 2014) and *Mt*LPMO9E (*Mt*LPMO9J) (Kadowaki et al., 2018; Sun, Laurent, et al., 2020), all having a similar active site configuration ($^{-}$Seg1^{+}Seg2). *Mt*LPMO9H, on the other hand, only showed cleavage towards xyloglucan next to oxidative cleavage of cellulosic substrates (Fig. 1).

Next, we studied the xyloglucan cleavage by *Mt*LPMO9H and *Mt*LPMO9F in further detail. As predicted, oxidative cleavage of xyloglucan, and distinct product profiles were observed (Fig. 1). Both enzymes were free of xyloglucanase impurity (Fig. A.6).

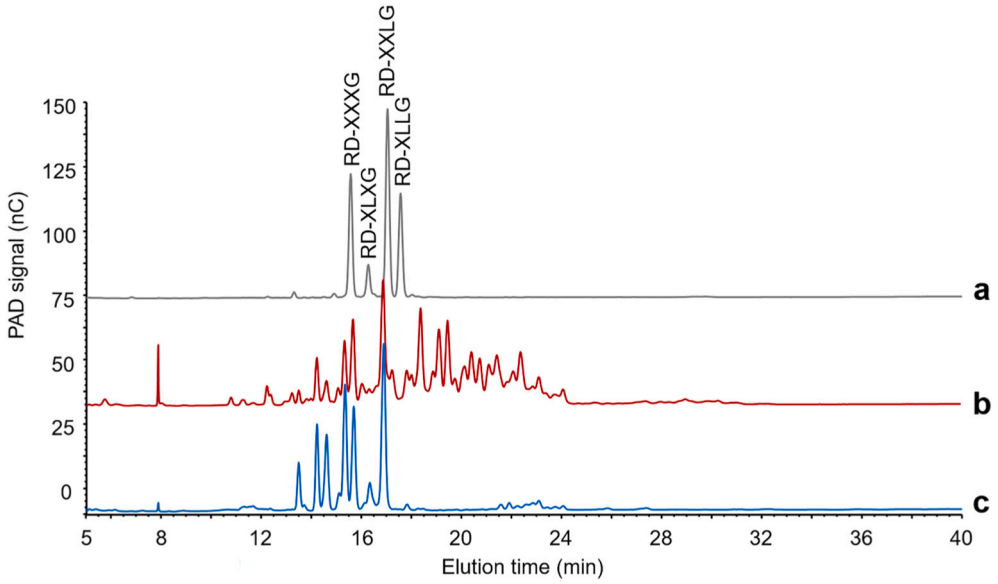

Fig. 2. HPAEC chromatograms of *Mt*LPMO9H- and *Mt*LPMO9F-TXG digests after $NaBD_4$-reduction. (a) Reduced TXG oligosaccharide standard mixture (RD-XXXG, RD-XLXG, RD-XXLG and RD-XLLG); (b) *Mt*LPMO9H-TXG digest in the presence of Asc; (c) *Mt*LPMO9F-TXG digest in the presence of Asc.

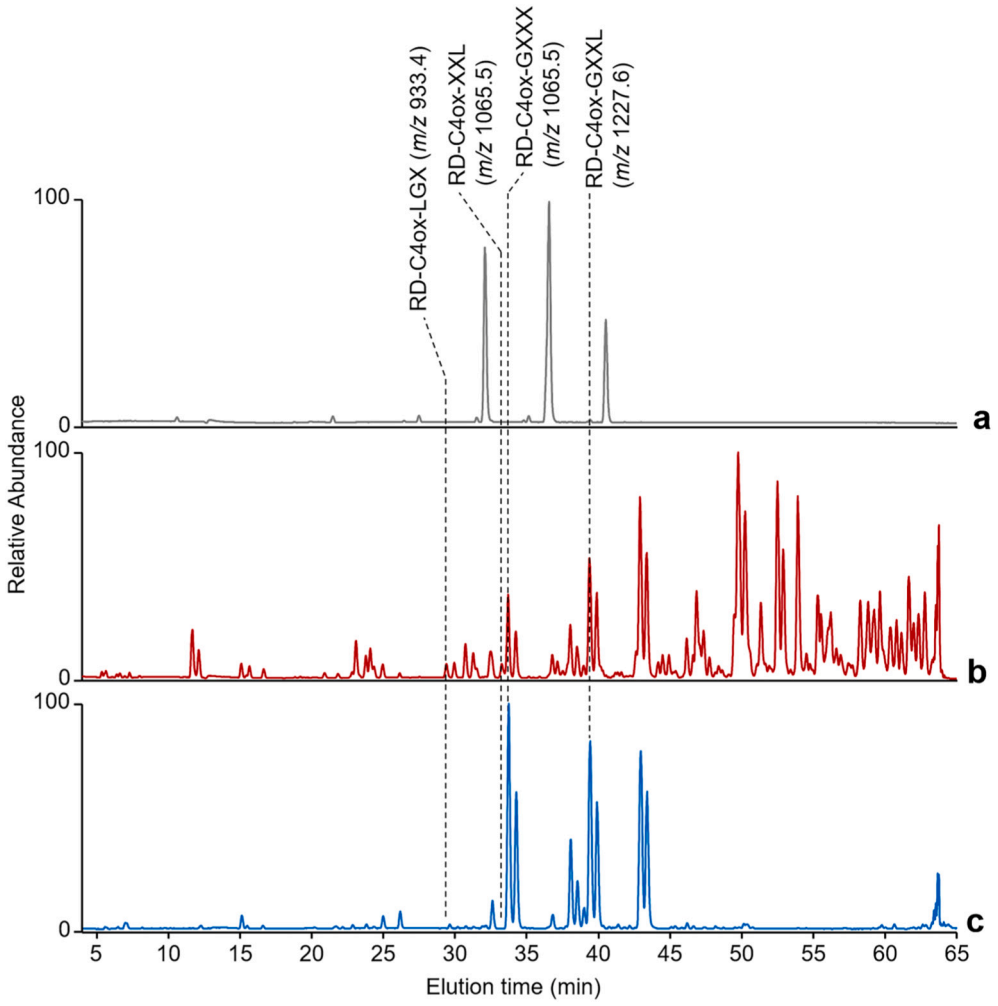

Fig. 3. HILIC-ESI-MS base-peak chromatograms. (a) Reduced TXG oligosaccharide standard mixture; (b) *Mt*LPMO9H-TXG digest in the presence of Asc; (c) *Mt*LPMO9F-TXG digest in the presence of Asc.

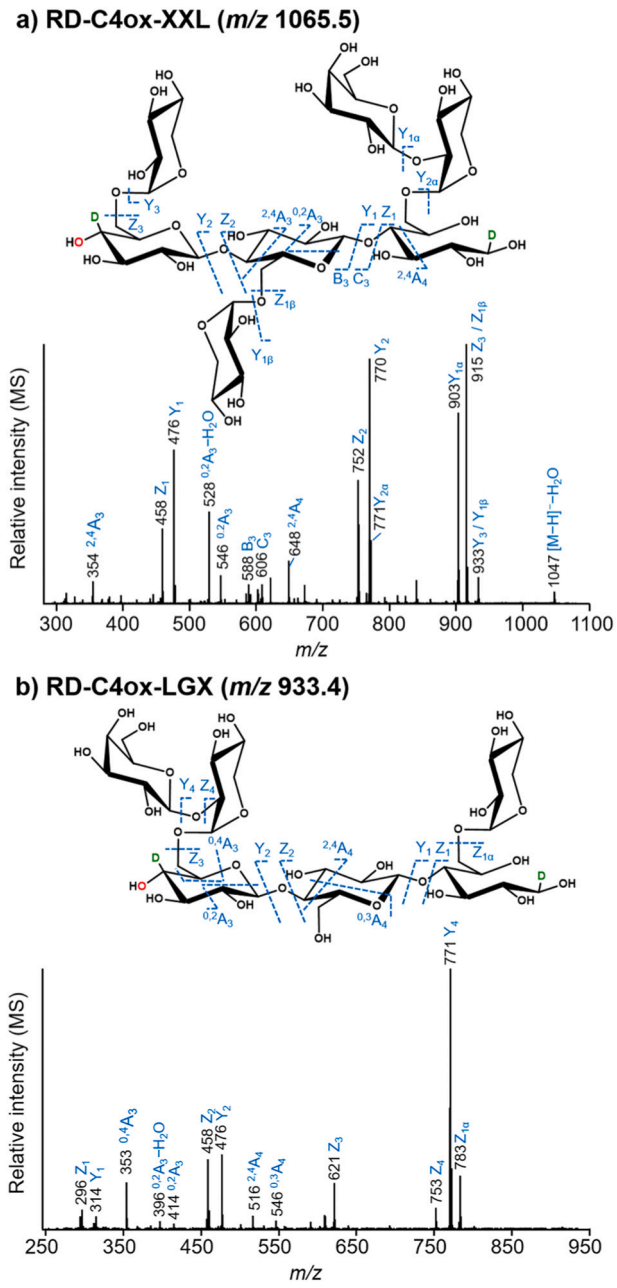

Fig. 4. Negative ion mode CID-MS^2 fragmentation patterns of reduced C4-oxidized TXG oligosaccharide. (a) RD-C4ox-XXL (*m/z* 1065.6) and (b) RD-C4ox-LGX (*m/z* 933.4). Only the structures with glucosyl non-reducing end were used to demonstrate their structural elucidation.

3.2. Xyloglucan cleavage profiles of MtLPMO9H and MtLPMO9F correlate to their active site segment configuration

To further map detailed xyloglucan product profiles generated by *Mt*LPMO9H and *Mt*LPMO9F, the corresponding digests were reduced by using $NaBD_4$ and subjected to HPAEC (Fig. 2) and HILIC-ESI-CID-MS/MS^2 (Fig. 3). In HPAEC chromatograms of the reduced TXG digests, again different TXG oligosaccharide profiles were observed for *Mt*LPMO9H (Fig. 2b), and *Mt*LPMO9F (Fig. 2c).

Similar to the HPAEC data, the HILIC-ESI-MS base-peak chromatograms of the two digests were different (Fig. 3). The reduction significantly improved the separation, especially of C4-oxidized TXG oligosaccharides in HILIC, compared to the previously reported non-reduced ones (Sun, Laurent, et al., 2020). Nevertheless, a drawback of reduction of C4-oxidized oligosaccharides (RD-C4ox) is that both glucosyl and galactosyl non-reducing ends are formed (Sun, Frommhagen, et al., 2020), depending whether the hydroxyl group adds in axial or equatorial position to the C4 of the non-reducing end. Unfortunately, these reduced "corresponding" couples (e.g., reduced C4-oxidized TXG-products) were not well separated in HILIC, and comprise the same *m/z*. Therefore, in the further characterization, glucosyl or galactosyl non-reducing ends were not further distinguished. On the basis of *m/z* values and corresponding MS^2 fragmentation patterns, multiple reduced C4-oxidized TXG oligosaccharides were identified. In particular, for the *Mt*LPMO9H-TXG digest, originally C4-oxidized TXG oligomers having the C4-oxidation at their non-reducing X unit (e.g., RD-C4ox-XG (*m/z* 477.3), RD-C4ox-XX (*m/z* 609.3), RD-C4ox-XXL (*m/z* 1065.5; Fig. 4a)),

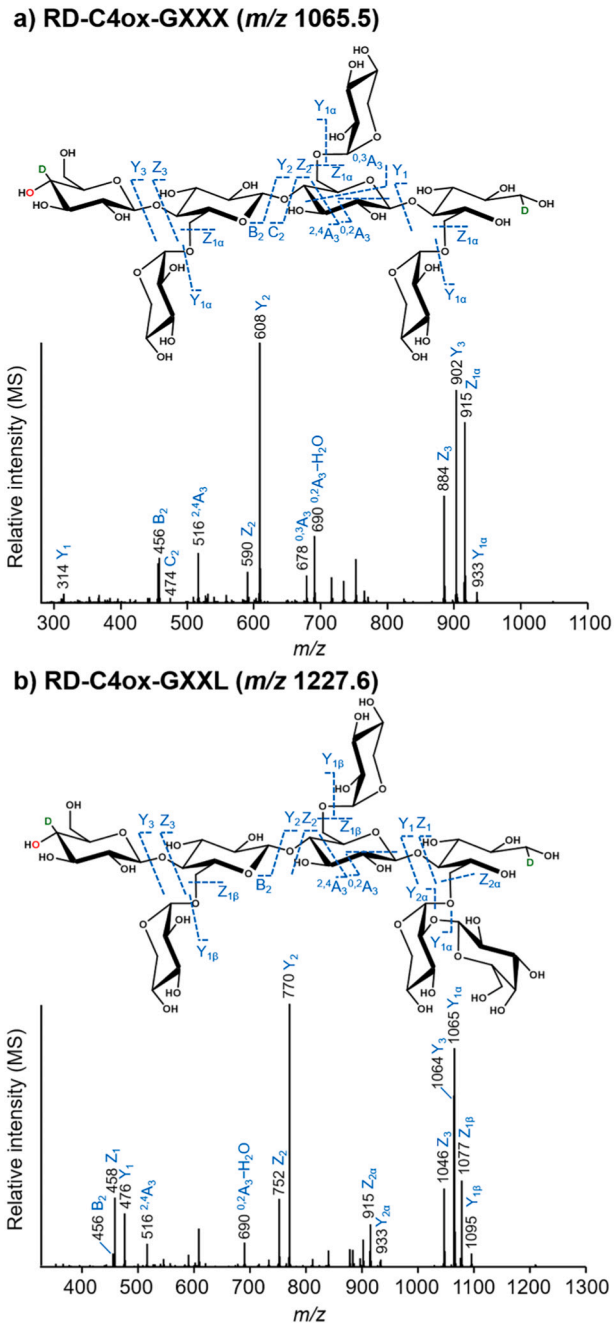

Fig. 5. Negative ion mode CID-MS^2 fragmentation patterns of reduced C4-oxidized TXG oligosaccharide. (a) RD-C4ox-GXXX (*m/z* 1065.5) and (b) RD-C4ox-GXXL (*m/z* 1227.6). Only the structures with glucosyl non-reducing end were used to demonstrate their structural elucidation.

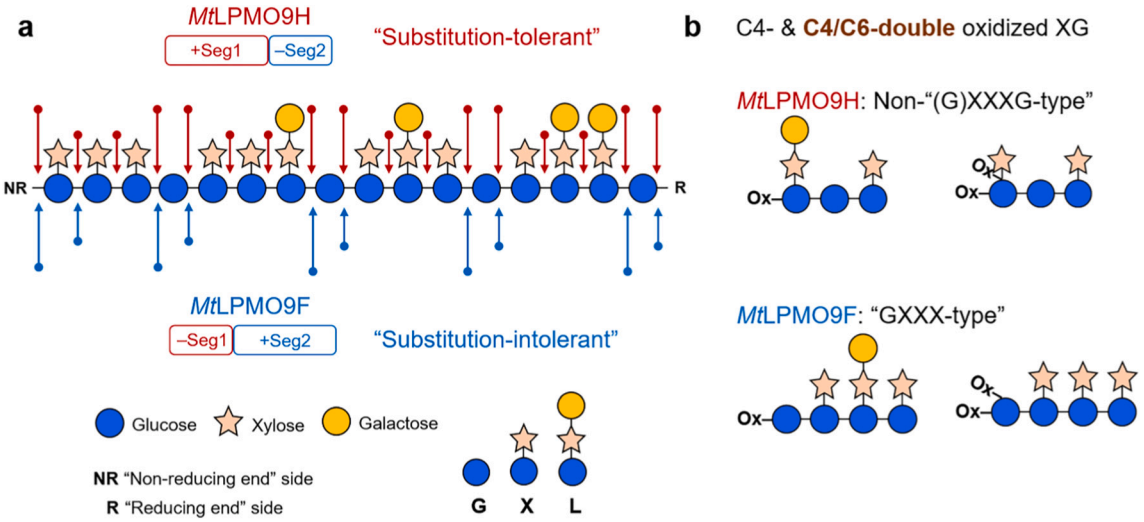

Fig. 6. Schematic representation of TXG cleavage patterns by *Mt*LPMO9H (a, red arrows) and *Mt*LPMO9F (a, blue arrows), respectively. *Mt*LPMO9H oxidatively cleaved XG regardless of substitution (substitution-tolerant) with seemingly preference on unsubstituted glucosyl units. *Mt*LPMO9F showed "substitution-intolerant" cleavage pattern meaning that its oxidative cleavage towards XG was predominately at the non-reducing end of unbranched glucosyl residues. The size of the arrows is indicative for more pronounced cleavage sites. (b) Schematic structural illustration of C4- and C4/C6-double oxidized TXG oligosaccharides released by *Mt*LPMO9H (top, non-"(G)XXXG-type") and *Mt*LPMO9F (bottom, "GXXX-type"). Ox: oxidized position. (For interpretation of the references to color in this figure legend, the reader is referred to the web version of this article.)

and at their non-reducing L unit (e.g., RD-C4ox-LGX (*m/z* 933.4; Fig. 4b)) were identified. All these products are evident for TXG "substitution-tolerant" cleavage, and these products were absent in the reduced *Mt*LPMO9F-TXG digest.

To briefly explain the structural identification shown in Fig. 4a, for RD-C4ox-XXL (*m/z* 1065, $[M–H]^-$), predominantly Y- and Z-type fragments were found, including Y_2 (*m/z* 770), Z_2 (*m/z* 752), Y_1 (*m/z* 476) and Z_1 (*m/z* 458). These fragments, especially Y_2 and Z_2, indicated a loss of a reduced C4-oxidized X unit. The *m/z* difference of 294, from Y_2 to Y_1 and Z_2 to Z_1, indicated an internal X unit, situated directly next to the reduced C4-oxidized X unit. The reduced C4-oxidized X unit was further confirmed by the fragments from cross-ring cleavage including $^{2,4}A_3$ (*m/z* 354), $^{0,2}A_3$ ($–H_2O$) (*m/z* 546 and 528) and $^{2,4}A_4$ (*m/z* 648). The *m/z* difference of 162 and 294 compared $Y_{1\alpha}$ (*m/z* 903) and $Y_{2\alpha}$ (*m/z* 771) to the parent *m/z* (1065.5), respectively, and confirmed the final structure of RD-C4ox-XXL, but not the isomeric RD-C4ox-XXXG. In addition, $Y_{1\alpha}$ (*m/z* 903) and $Y_{2\alpha}$ (*m/z* 771) ions were diagnostic fragments representing the loss of non-deuterium-added hexaosyl (H_1P_0) and hexaosyl + pentaosyl (H_1P_1) units, respectively, which cannot be generated from the RD-C4ox-XXXG structure, and thus again confirmed the RD-C4ox-XXL structure.

For RD-C4ox-LGX (*m/z* 933.4, $[M–H]^-$), having a reduced C4-oxidized L unit, identification was similar as described above (Fig. 4b). Fragmentation of RD-C4ox-LGX MS^2 showed as main fragments Y_2 (*m/z* 476), Z_2 (*m/z* 458), $^{0,2}A_3$ ($-H_2O$) (*m/z* 414 and 396) and $^{2,4}A_4$ (*m/z* 516). However, these four fragments can also represent the reduced C4-oxidized "GX" or "XG" in addition to the "L" unit (all three are H_2P_1). The L unit was determined to be at the non-reducing end side based on: i) Y_4 (*m/z* 771), Z_4 (*m/z* 753) and $^{0,4}A_3$ (*m/z* 353) ions representing the loss of non-deuterium-added hexaosyl units (H_1P_0, *m/z* loss of 162 or 180). This *m/z* loss confirms the presence of a galactosyl unit but not a glucosyl unit, as terminal glucosyl units either have one deuterium in the non-reducing end (*m/z* loss of 163 or 181) or in the reducing end of an alditol form (*m/z* loss of 165 or 183). ii) Y_1 (*m/z* 314) and Z_1 (*m/z* 296) fragments suggested that an X unit was present in the alditol form of a reducing end side, and thus the galactosyl unit can only be present in the middle or at the non-reducing end. iii) Taken into account the parental *m/z* value (representing the H_4P_2 structure) and the TXG structure ("XXXG-type" building blocks), the L unit can only be present at the non-reducing end.

Other non-"XXXG-type" TXG oligosaccharides (DP > 9; *m/z* > 1389.7) eluted after 45 min (Fig. 3) in the *Mt*LPMO9H-TXG digest again indicative for a "substitution-tolerant" cleavage. Due to the complexity, their exact structures have not been elucidated further.

In the reduced *Mt*LPMO9F-TXG digest, several originally C4-oxidized "GXXX-type" building blocks were identified, for example RD-C4ox-GXXX and RD-C4ox-GXXL (Fig. 3). In the MS^2 spectrum of RD-C4ox-GXXX (*m/z* 1065.5, $[M–H]^-$, Fig. 5a), Y_3 (*m/z* 902) and Z_3 (*m/z* 884) fragments indicated the loss of the reduced C4-oxidized G unit from the non-reducing end. The absence of an ion with *m/z* of 903 (difference of 162 compared to the parent *m/z*) suggested the absence of a galactosyl unit, as described above. In addition, other fragments from either β-(1→4)-glycosidic bond cleavage (Y_1, *m/z* 314; B_2, *m/z* 456; C_2, *m/z* 474; Z_2, *m/z* 590 and Y_2, *m/z* 608) or cross-ring cleavage ($^{2,4}A_3$, *m/z* 516; $^{0,3}A_3$, *m/z* 678 and $^{0,2}A_3–H_2O$, *m/z* 690) further confirmed the structure of RD-C4ox-GXXX. RD-C4ox-GXXL (*m/z* 1227.6, $[M–H]^-$, Fig. 5b) was identified in a similar way as described for RD-C4ox-GXXX. The diagnostic fragments $Y_{1\alpha}$ (*m/z* 1065) and Y_3 (*m/z* 1064) represented the loss of a reduced C4-oxidized G unit from the non-reducing end and a galactosyl unit, respectively. Other fragments originating from either β-(1→4)-glycosidic bond cleavage (B_2, *m/z* 456; Z_1, *m/z* 458; Y_1, *m/z* 476; Z_2, *m/z* 752 and Y_2, *m/z* 770) or cross-ring cleavage ($^{2,4}A_3$, *m/z* 516 and $^{0,2}A_3–H_2O$, *m/z* 690) further reflected the structure of RD-C4ox-GXXL. These identified "GXXX-type" C4-oxidized TXG oligosaccharides, together with the absence of non-"XXXG-type" ones, suggested a "substitution-intolerant" cleavage of TXG by *Mt*LPMO9F (Fig. 6). Notably, the "GXXX-type" C4-oxidized TXG oligosaccharides were also present in the *Mt*LPMO9H-TXG digest (Fig. 4), which may indicate that *Mt*LPMO9H preferably cleaved at the "non-reducing end" site of the G unit, though cleavage next to a substituted glucosyl unit was also identified to occur (Fig. 6). This preference of *Mt*LPMO9H differs from the previously characterized *Nc*LPMO9M, which has been shown to preferentially cleave next to substituted glucosyl units (Sun, Laurent, et al., 2020). It is speculated that this preference difference is caused by the presence of a carbohydrate binding module 1 (CBM1) in *Mt*LPMO9H, but not in *Nc*LPMO9M. CBM1 could influence the binding of the LPMO catalytic domain to the xyloglucan polymer, and thus partially alter the cleavage preference of *Mt*LPMO9H.

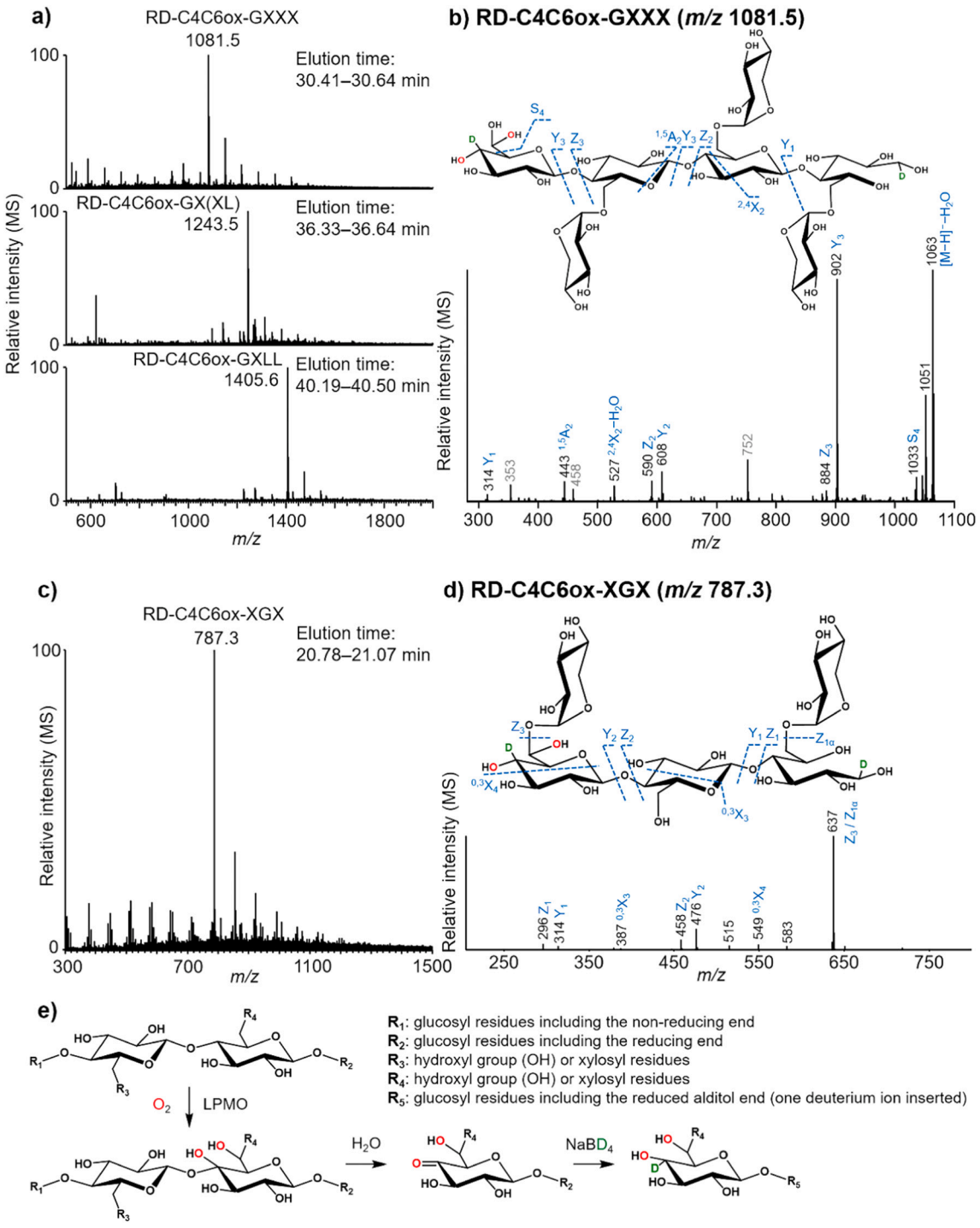

Fig. 7. Negative ion mode HILIC-ESI-MS and CID-MS^2 spectra of multiple reduced C4/C6-double oxidized TXG oligosaccharides and proposed route for the xyloglucan-active LPMO-catalyzed generation of C4/C6-double oxidized TXG oligosaccharides. (a) MS spectra of *m/z* 1081.5 (elution time 30.41–30.64 min), *m/z* 1243.5 (elution time 36.33–36.64 min) and *m/z* 1405.6 (elution time 40.19–40.50 min), from top to bottom. (b) Negative ion mode CID-MS^2 fragmentation patterns of reduced C4/C6-double oxidized TXG oligosaccharide RD-C4C6ox-GXXX (*m/z* 1081.5). Fragments in grey color are tentatively proposed to be from other isomeric structures. (c) MS spectrum of *m/z* 787.3 (elution time 20.78–21.07 min). (d) Negative ion mode CID-MS^2 fragmentation patterns of reduced C4/C6-double oxidized TXG oligosaccharide RD-C4C6ox-XGX (*m/z* 787.3). (e) Proposed route for the LPMO-catalyzed generation of C4/C6-double oxidized TXG oligosaccharides as supported by $NaBD_4$ reduction experiments.

3.3. MtLPMO9H and MtLPMO9F generates C4/C6-double oxidized xylogluco-oligosaccharides

In addition to reduced C4-oxidized TXG oligosaccharides, reduced C4/C6-double oxidized TXG oligosaccharides were identified (Figs. 6 and 7). Fig. 7a shows the full MS spectra of RD-C4C6ox-GXXX (*m/z* 1081.5, [M–H]$^-$), RD-C4C6ox-GX(XL) (*m/z* 1243.5, [M–H]$^-$) and RD-C4C6ox-GXLL (*m/z* 1405.6, [M–H]$^-$) detected in the *Mt*LPMO9F-TXG digest (also present in the *Mt*LPMO9H-TXG digest, but to a lesser extent (not shown)). The RD-C4C6ox-GXXX MS^2 spectrum (*m/z* 1081.5, [M–H]$^-$, Fig. 7b) is used as an example to demonstrate our structural elucidation. First, the reduced C4/C6-double oxidized unsubstituted

glucosyl unit at the non-reducing end was identified by the *m/z* difference of 179 and 197, from Y_3 (*m/z* 902) and Z_3 (*m/z* 884) compared to the parent *m/z* (1081.5), respectively. The novel S-type ion (S_4, *m/z* 1033), that indicates the loss of a C6-gem-diol structure in reduced C4/C6 double oxidized cello-oligosaccharides (Sun et al., 2022), was also found here. Other fragments, including Y_2 (*m/z* 314), $^{1,5}A_2$ (*m/z* 433), $^{2,4}A_2$ (*m/z* 527), Z_3 (*m/z* 590) and Y_3 (*m/z* 608), indicated the loss of a reduced unsubstituted glucosyl unit originally having a C4-ketone and C6-gem-diol moiety at the non-reducing end, further confirmed the structure of RD-C4C6ox-GXXX. Our previous study demonstrated that the C6-gem-diol moiety in the C4/C6-double oxidized cello-oligosaccharides is formed via the oxygenation reaction of LPMOs, though the oxidation to C6-aldehyde followed by hydration to C6-gem-diol could not be excluded (Sun et al., 2022). Notably, in the RD-C4C6ox-GXXX MS^2 spectrum, several less abundant fragments (*m/z* 353, 458 and 752) were detected, which were, possibly, from the isomeric structure RD-C4C6ox-X(H_3P_2) (*m/z* 1081.5, $[M–H]^-$). As in these structures the C6-carbon atom is substituted with a xylosyl unit at the non-reducing end G, C6-oxidation can here only occur via the oxygenation reaction, and direct oxidation to a C6-aldehyde would not be possible. In line with its substitution-tolerant cleavage behavior, *Mt*LPMO9H generated a different C4/C6-double oxidized XGX unit (RD-C4C6ox-XGX, *m/z* 787.3, $[M–H]^-$, Fig. 7c). Based on the MS and MS^2 spectra (Fig. 7d), insertion of a hydroxyl group on the substituted C6 atom was found in RD-C4C6ox-XGX. Therefore, we conclude that C6-oxidation of xyloglucan by AA9 LPMOs follows the oxygenation route, and does not occur via direct oxidation (Fig. 7e).

4. Conclusions

In this study, we characterized two AA9 *Mt*LPMOs, having different active site segments, for their regioselectivity and xyloglucan cleavage profiles. We found that *Mt*LPMO9F and *Mt*LPMO9H both oxidatively cleaved cellulose and xyloglucan, while *Mt*LPMO9F even displayed a broader substrate specificity. Using $NaBD_4$-reduction followed by HILIC-ESI-CID-MS/MS^2 analysis, we showed that *Mt*LPMO9F released majorly C4-oxidized cello-oligosaccharides and C4/C6-double oxidized ones. In addition, C4/C6-double oxidized xylogluco-oligosaccharides were detected and formed via an oxygenation reaction. We further revealed that *Mt*LPMO9H ($^+$Seg1$^-$Seg2) displayed xyloglucan "substitution-tolerant" cleavages, while *Mt*LPMO9F ($^-$Seg1$^+$Seg2) displayed xyloglucan "substitution-intolerant" cleavages. These findings support the hypothesis that the configuration of active site segments in AA9 LPMOs can be used to predict their xyloglucan cleavage profiles.

CRediT authorship contribution statement

Peicheng Sun: Conceptualization, Data curation, Formal analysis, Investigation, Methodology, Software, Validation, Visualization, Writing – original draft. **Melanie de Munnik:** Data curation, Formal analysis, Investigation, Methodology, Writing – review & editing. **Willem J.H. van Berkel:** Conceptualization, Investigation, Supervision, Validation, Writing – review & editing. **Mirjam A. Kabel:** Conceptualization, Funding acquisition, Investigation, Project administration, Resources, Supervision, Validation, Visualization, Writing – original draft, Writing – review & editing.

Declaration of competing interest

The authors declare that they have no known competing financial interests or personal relationships that could have appeared to influence the work reported in this paper.

Acknowledgements

The authors thank Sandra W.A. Hinz and Martijn J. Koetsier for their help in producing the LPMO enzymes (IFF Nutrition & Biosciences). Mark G. Sanders and Margaret Bosveld (Wageningen University & Research) are acknowledged for their help with HILIC-ESI-CID-MS/MS^2 and HPAEC, respectively. We gratefully thank Madelon Logtenberg, Dimitrios Kouzounis and Henk A. Schols (Wageningen University & Research) for discussion.

Funding

This research did not receive any specific grant from funding agencies in the public, commercial, or not-for-profit sectors.

Appendix A. Supplementary data

Supplementary data to this article can be found online at https://doi.org/10.1016/j.carbpol.2022.119373.

References

Agger, J. W., Isaksen, T., Varnai, A., Vidal-Melgosa, S., Willats, W. G., Ludwig, R., & Westereng, B. (2014). Discovery of LPMO activity on hemicelluloses shows the importance of oxidative processes in plant cell wall degradation. *Proceedings of the National Academy of Sciences of the United States of America, 111*, 6287–6292.

Beeson, W. T., Phillips, C. M., Cate, J. H., & Marletta, M. A. (2012). Oxidative cleavage of cellulose by fungal copper-dependent polysaccharide monooxygenases. *Journal of the American Chemical Society, 134*, 890–892.

Berka, R. M., Grigoriev, I. V., Otillar, R., Salamov, A., Grimwood, J., Reid, I., & Moisan, M.-C. (2011). Comparative genomic analysis of the thermophilic biomass-degrading fungi *Myceliophthora thermophila* and *Thielavia terrestris*. *Nature Biotechnology, 29*, 922–927.

Bissaro, B., Varnai, A., Rohr, A. K., & Eijsink, V. G. H. (2018). Oxidoreductases and reactive oxygen species in conversion of lignocellulosic biomass. *Microbiology and Molecular Biology Reviews, 82*. e00029-00018.

Caffall, K. H., & Mohnen, D. (2009). The structure, function, and biosynthesis of plant cell wall pectic polysaccharides. *Carbohydrate Research, 344*, 1879–1900.

Cannella, D., Chia-wen, C. H., Felby, C., & Jørgensen, H. (2012). Production and effect of aldonic acids during enzymatic hydrolysis of lignocellulose at high dry matter content. *Biotechnology for Biofuels, 5*, 1–10.

Chen, K., Zhang, X., Long, L., & Ding, S. (2021). Comparison of C4-oxidizing and C1/C4-oxidizing AA9 LPMOs in substrate adsorption, H_2O_2-driven activity and synergy with cellulase on celluloses of different crystallinity. *Carbohydrate Polymers, 269*, Article 118305.

Cherubini, F. (2010). The biorefinery concept: Using biomass instead of oil for producing energy and chemicals. *Energy Conversion and Management, 51*, 1412–1421.

Forsberg, Z., Vaaje-Kolstad, G., Westereng, B., Bunaes, A. C., Stenstrom, Y., MacKenzie, A., & Eijsink, V. G. H. (2011). Cleavage of cellulose by a CBM33 protein. *Protein Science, 20*, 1479–1483.

Frandsen, K. E., & Lo Leggio, L. (2016). Lytic polysaccharide monooxygenases: A crystallographer's view on a new class of biomass-degrading enzymes. *IUCrJ, 3*, 448–467.

Frommhagen, M., Koetsier, M. J., Westphal, A. H., Visser, J., Hinz, S. W. A., Vincken, J.-P., & Gruppen, H. (2016). Lytic polysaccharide monooxygenases from *Myceliophthora thermophila* C1 differ in substrate preference and reducing agent specificity. *Biotechnology for Biofuels, 9*, 186.

Frommhagen, M., Sforza, S., Westphal, A. H., Visser, J., Hinz, S. W., Koetsier, M. J., & Kabel, M. A. (2015). Discovery of the combined oxidative cleavage of plant xylan and cellulose by a new fungal polysaccharide monooxygenase. *Biotechnology for Biofuels, 8*, 101.

Frommhagen, M., van Erven, G., Sanders, M., van Berkel, W. J. H., Kabel, M. A., & Gruppen, H. (2017a). RP-UHPLC-UV-ESI-MS/MS analysis of LPMO generated C4-oxidized gluco-oligosaccharides after non-reductive labeling with 2-aminobenzamide. *Carbohydrate Research, 448*, 191–199.

Frommhagen, M., Westphal, A. H., Hilgers, R., Koetsier, M. J., Hinz, S. W. A., Visser, J., & Kabel, M. A. (2017b). Quantification of the catalytic performance of C1-cellulose-specific lytic polysaccharide monooxygenases. *Applied Microbiology and Biotechnology, 102*, 1281–1295.

Fry, S. C., York, W. S., Albersheim, P., Darvill, A., Hayashi, T., Joseleau, J. P., & McNeil, M. (1993). An unambiguous nomenclature for xyloglucan-derived oligosaccharides. *Physiologia Plantarum, 89*, 1–3.

Gao, D. H., Uppugundla, N., Chundawat, S. P. S., Yu, X. R., Hermanson, S., Gowda, K., & Dale, B. E. (2011). Hemicellulases and auxiliary enzymes for improved conversion of lignocellulosic biomass to monosaccharides. *Biotechnology for Biofuels, 4*, 5.

Grieco, M. A. B., Haon, M., Grisel, S., de Oliveira-Carvalho, A. L., Magalhaes, A. V., Zingali, R. B., & Berrin, J. G. (2020). Evaluation of the enzymatic arsenal secreted by *Myceliophthora thermophila* during growth on sugarcane bagasse with a focus on LPMOs. *Frontiers in Bioengineering and Biotechnology, 8*, 1028.

Hangasky, J. A., Iavarone, A. T., & Marletta, M. A. (2018). Reactivity of O_2 versus H_2O_2 with polysaccharide monooxygenases. *Proceedings of the National Academy of Sciences of the United States of America, 115*, 4915–4920.

Harris, P. V., Welner, D., McFarland, K., Re, E., Navarro Poulsen, J.-C., Brown, K., & Merino, S. (2010). Stimulation of lignocellulosic biomass hydrolysis by proteins of glycoside hydrolase family 61: Structure and function of a large, enigmatic family. *Biochemistry, 49*, 3305–3316.

Himmel, M. E., Ding, S. Y., Johnson, D. K., Adney, W. S., Nimlos, M. R., Brady, J. W., & Foust, T. D. (2007). Biomass recalcitrance: Engineering plants and enzymes for biofuels production. *Science, 315*, 804–807.

Hinz, S. W., Pouvreau, L., Joosten, R., Bartels, J., Jonathan, M. C., Wery, J., & Schols, H. A. (2009). Hemicellulase production in *Chrysosporium lucknowense* C1. *Journal of Cereal Science, 50*, 318–323.

Hoffman, M., Jia, Z., Peña, M. J., Cash, M., Harper, A., Blackburn, A. R., II, & York, W. S. (2005). Structural analysis of xyloglucans in the primary cell walls of plants in the subclass Asteridae. *Carbohydrate Research, 340*, 1826–1840.

Isaksen, T., Westereng, B., Aachmann, F. L., Agger, J. W., Kracher, D., Kittl, R., & Horn, S. J. (2014). A C4-oxidizing lytic polysaccharide monooxygenase cleaving both cellulose and cello-oligosaccharides. *Journal of Biological Chemistry, 289*, 2632–2642.

Kadowaki, M. A., Várnai, A., Jameson, J.-K., Leite, A. E., Costa-Filho, A. J., Kumagai, P. S., & Eijsink, V. G. (2018). Functional characterization of a lytic polysaccharide monooxygenase from the thermophilic fungus *Myceliophthora thermophila*. *PLOS One, 13*, Article e0202148.

Karnaouri, A., Muraleedharan, M. N., Dimarogona, M., Topakas, E., Rova, U., Sandgren, M., & Christakopoulos, P. (2017). Recombinant expression of thermostable processive *Mt*EG5 endoglucanase and its synergism with *Mt*LPMO from *Myceliophthora thermophila* during the hydrolysis of lignocellulosic substrates. *Biotechnology for Biofuels, 10*, 126.

Laurent, C. V. F. P., Sun, P., Scheiblbrandner, S., Csarman, F., Cannazza, P., Frommhagen, M., & Ludwig, R. (2019). Influence of lytic polysaccharide monooxygenase active site segments on activity and affinity. *International Journal of Molecular Sciences, 20*, 6219.

Lombard, V., Ramulu, H. G., Drula, E., Coutinho, P. M., & Henrissat, B. (2014). The carbohydrate-active enzymes database (CAZy) in 2013. *Nucleic Acids Research, 42*, D490–D495.

McNeil, M., Darvill, A. G., Fry, S. C., & Albersheim, P. (1984). Structure and function of the primary cell walls of plants. *Annual Review of Biochemistry, 53*, 625–663.

Merino, S. T., & Cherry, J. (2007). Progress and challenges in enzyme development for biomass utilization. *Biofuels, 108*, 95–120.

Monclaro, A. V., Petrović, D. M., Alves, G. S., Costa, M. M., Midorikawa, G. E., Miller, R. N., & Várnai, A. (2020). Characterization of two family AA9 LPMOs from *Aspergillus tamarii* with distinct activities on xyloglucan reveals structural differences linked to cleavage specificity. *PLOS One, 15*, Article e0235642.

Nanda, S., Mohammad, J., Reddy, S. N., Kozinski, J. A., & Dalai, A. K. (2014). Pathways of lignocellulosic biomass conversion to renewable fuels. *Biomass Conversion and Biorefinery, 4*, 157–191.

Nekiunaite, L., Petrovic, D. M., Westereng, B., Vaaje-Kolstad, G., Hachem, M. A., Varnai, A., & Eijsink, V. G. (2016). *Fg*LPMO9A from *Fusarium graminearum* cleaves xyloglucan independently of the backbone substitution pattern. *FEBS Letters, 590*, 3346–3356.

Payne, C. M., Knott, B. C., Mayes, H. B., Hansson, H., Himmel, M. E., Sandgren, M., & Beckham, G. T. (2015). Fungal cellulases. *Chemical Reviews, 115*, 1308–1448.

Punt, P. J., Burlingame, R. P., Pynnonen, C. M., Olson, P. T., Wery, J., Visser, J., & Verdoes, J. (2010). Chrysosporium lucknowense protein production system. In *, Vol. 2. World Intellectual Property Organization patent*.

Sabbadin, F., Urresti, S., Henrissat, B., Avrova, A. O., Welsh, L. R. J., Lindley, P. J., & McQueen-Mason, S. J. (2021). Secreted pectin monooxygenases drive plant infection by pathogenic oomycetes. *Science, 373*, 774.

Simmons, T. J., Frandsen, K. E. H., Ciano, L., Tryfona, T., Lenfant, N., Poulsen, J. C., & Dupree, P. (2017). Structural and electronic determinants of lytic polysaccharide monooxygenase reactivity on polysaccharide substrates. *Nature Communications, 8*, 1064.

Straathof, A. J. (2014). Transformation of biomass into commodity chemicals using enzymes or cells. *Chemical Reviews, 114*, 1871–1908.

Sun, P., Frommhagen, M., Kleine Haar, M., van Erven, G., Bakx, E. J., van Berkel, W. J. H., & Kabel, M. A. (2020a). Mass spectrometric fragmentation patterns discriminate C1- and C4-oxidised cello-oligosaccharides from their non-oxidised and reduced forms. *Carbohydrate Polymers, 234*, Article 115917.

Sun, P., Laurent, C. V. F. P., Boerkamp, V. J. P., van Erven, G., Ludwig, R., van Berkel, W. J. H., & Kabel, M. A. (2022). Regioselective C4 and C6 double oxidation of cellulose by lytic polysaccharide monooxygenases. *ChemSusChem, 15*, Article e202102203.

Sun, P., Laurent, C. V. F. P., Scheiblbrandner, S., Frommhagen, M., Kouzounis, D., Sanders, M. G., & Kabel, M. A. (2020b). Configuration of active site segments in lytic polysaccharide monooxygenases steers oxidative xyloglucan degradation. *Biotechnology for Biofuels, 13*, 95.

Sun, P., Valenzuela, S. V., Chunkrua, P., Pastor, F. I. J., Laurent, C. V. F. P., Ludwig, R., & Kabel, M. A. (2021). Oxidized product profiles of AA9 lytic polysaccharide monooxygenases depend on the type of cellulose. *ACS Sustainable Chemistry & Engineering, 9*, 14124–14133.

Vaaje-Kolstad, G., Forsberg, Z., Loose, J. S., Bissaro, B., & Eijsink, V. G. (2017). Structural diversity of lytic polysaccharide monooxygenases. *Current Opinion in Structural Biology, 44*, 67–76.

Vincken, J. P., York, W. S., Beldman, G., & Voragen, A. G. (1997). Two general branching patterns of xyloglucan, XXXG and XXGG. *Plant Physiology, 114*, 9–13.

Visser, H., Joosten, V., Punt, P. J., Gusakov, A. V., Olson, P. T., Joosten, R., & Emalfarb, M. A. (2011). Development of a mature fungal technology and production platform for industrial enzymes based on a *Myceliophthora thermophila* isolate, previously known as *Chrysosporium lucknowense* C1. *Industrial Biotechnology, 7*, 214–223.

Vu, V. V., Beeson, W. T., Phillips, C. M., Cate, J. H., & Marletta, M. A. (2014). Determinants of regioselective hydroxylation in the fungal polysaccharide monooxygenases. *Journal of the American Chemical Society, 136*, 562–565.

Zhou, H., Li, T., Yu, Z., Ju, J., Zhang, H., Tan, H., & Yin, H. (2019). A lytic polysaccharide monooxygenase from *Myceliophthora thermophila* and its synergism with cellobiohydrolases in cellulose hydrolysis. *International Journal of Biological Macromolecules, 139*, 570–576.